EFDA–JET–CP(03)01-52

V Riccardo and JET EFDA Contributors

Disruptions and Disruption Mitigation

Disruptions and Disruption Mitigation

V Riccardo
and JET EFDA Contributors*

EURATOM/UKAEA Fusion Association, Culham Science Centre, Abingdon,OX14 3DB, UK
See Annex of J. Pamela et al., "Overview of Recent JET Results and Future Perspectives",
Fusion Energy 2000 (Proc. 18th Int. Conf. Sorrento, 2000), IAEA, Vienna (2001).

ABSTRACT.

Detailed disruption related studies have been undertaken at JET in 2001-3. An enhanced halo current detection system has allowed more precise halo asymmetry measurements to be made, confirming the assumptions in the ITER design guidelines. The runaway electron database has been systematically analysed and self–consistent simulations are underway. Disruption heat deposition, which is of fundamental importance for ITER, has been investigated and in JET it has been found that normally only a small fraction of the thermal energy goes to the divertor during the whole disruption. In addition, some energy has been observed on the outer wall at the thermal quench. The neutral point has been experimentally found and a plasma control model has been used to reproduce the dedicated discharges. Helium, neon and argon puffs have been applied as disruption mitigation techniques in JET following the success of recent studies in ASDEX Upgrade, TEXTOR and DIII-D.

1. INTRODUCTION

Plasma disruption is a sudden loss of magnetic confinement. The energy stored in the plasma is promptly released to the surrounding structures. Elongated plasma configurations lose vertical stability. When this occurs, the plasma contacts the wall and part of its current (halo) flows into them. Large toroidal voltage loop can accelerate runaway electrons, which may be lost to the vessel walls causing metallic components to melt.

Disruptions are likely to be unavoidable, at least on an occasional basis, in the operation of a tokamak. A better understanding of disruption loads is important, as they have a strong influence on the design of any new fusion device [1].

Since the beginning of 2001 JET has significantly progressed in the analysis of disruptions thanks to the installation of new hardware (refurbished halo current diagnostics) and with dedicated experiments (neutral point, runaway electron and disruption mitigation experiments) aimed at improving predictions and control methods for ITER.

The JET halo current diagnostics have recently been enhanced [2] allowing for better measurements of the toroidal peaking factor (TPF). The analysis of recently collected data is compared with those of MAST and ASDEX Upgrade in section 2.

Runaway electrons (REs) have systematically been produced in low elongation, limiter plasmas disrupted with impurity puffs. The ARENA code [3] has been used to self-consistent model the electron kinetics in one of these shots. Section 3 includes this numerical study and the discussion of the database.

Disruption heat loads are reported in section 4 and disruption mitigation results in section 5. The existence of a neutral point has been established for a small volume plasma subjected to radiative collapse. Its position has been reproduced using the CREATE_L linearized plasma response model [4]. Fast puffing of helium and higher-Z gases (neon and argon) was used to ameliorate disruptions. Due to limitations of the present JET gas injection system only halo currents could be reduced.

2. HALO CURRENT

The largest source of local stress on in-vessel components during disruptions is the poloidal current, which typically flows through the plasma scrape off layer, or halo, region and into plasma-facing surfaces. A good understanding of this source of disruption driven currents requires reliable measurements of the halo current. The technique employed in JET is to estimate the poloidal halo current from the variation of toroidal field within the halo current path outside the plasma.

Originally JET had two toroidal field pick-up coils at the top, and at the bottom, of the vessel in two locations set 180° apart. When the divertor structure was installed two additional toroidal field pick-up coils were incorporated. In addition a pair of instrumented protection tiles is fitted at the outer top of each octant and two poloidal voltage shunts in the divertor support structure [5]. Now only few of these probes are still working.

During the 2001 shutdown three Rogowski coils and three toroidal field pick-up coils have been installed together with the Improved Upper Inner Wall Protection (IUIWP) and two toroidal field pick-up coils in the divertor region.

The halo current Toroidal Peaking Factor (TPF) is defined as local maximum over the toroidal average and it is taken at the time of the maximum toroidally-averaged poloidal halo current. The halo current fraction is defined as the ratio of the maximum toroidally-averaged poloidal halo current to the pre-disruption plasma current. While with the two original measurement stations at 180° the n = 1 asymmetry TPF could be underestimated by 50%, with three at 90° it can only be underestimated only by 25%. The phase where the saturated kink mode locks during disruptions is not fixed, therefore over a large number of events the worst TPF could be captured. Figure 1 shows that the TPF measured by the IUIWP toroidal field pick-up coil in recent disruptions is not larger than it used to be. Figure 1 also contains the ITER reference design data for halo current [1]; the JET data are characterised by lower TPF than most of other machines. The typical design value of the product TPF times halo fraction, TPF·f, for ITER is 0.5, while 0.75 is the extreme value. Fig. 2 shows that for JET disruptions TPF·f is generally less than 0.5; the only event with TPF·f above 0.5 is a high-triangularity high-elongation deliberate VDE at low-q ($q_{95} < 2.5$). Figure 2 also shows that TPF·f does not depend on the plasma current, it depends instead on the qmin, the minimum value reached by the cylindrical approximation safety factor during the disruption: the largest TPF•f occur at small 4 q_{min}. Such qmin's are only reached when the 95-35% plasma current quench rate is slow (<100 MA/s).

To investigate the dependence on the pre-disruption safety factor a set of disruptions was triggered at constant plasma current and configuration but different boundary safety factor, q_{95}. No trend in the halo current magnitude or in the degree of asymmetry has been found. In fact, the I_p/q_{95} scaling proposed for the halo current data in Alcator C-mode data [6, 7] and supported by COMPASS-D data [8] does not fit JET data, nor DIII-D data [9], where large variations of halo current are observed at fixed I_p/q_{95}. The main cause for a deviation from the I_p/q_{95} scaling is the influence of the pre-disruption thermal content on the current decay rate [10]: high-bp disruptions are faster, maintain a

higher safety factor and have less poloidal halo current. This is evident in a dedicated set of bp–scan discharges. Two plasmas have been made vertically unstable by the control system when they had the same plasma current (2MA), the same boundary safety factor (~2.6), but different bp (0.18 and 0.48). The current decays more rapidly in the discharge with higher bp (125MA/s, compared to 75MA/s at low bp). Experimental data and simulations [11] show that the maximum poloidal halo current is larger in the discharge with lower β_p (500kA instead of 350kA).

The current collected by the IUIWP tiles is ~2% of total poloidal halo current, compatible with having 48 such supports, and the fact that the poloidal extent of the halo footprint is much smaller than these tiles. Figure 3 contains the traces of IUIWP Rogowski and pick-up coils and of an old pick-up coil located behind the dump plate. The Rogowski current peaks earlier than the current measured by the toroidal field pick-up coils. A plausible explanation for this is that the plasma moves along the vessel inner wall, which is also consistent with the plasma axis displacement (inwards and upwards) during the disruption. Initially, Fig.4(a), the IUIWP tiles collect current, but this current does not go around the pick-up coil, as it has to go to the wall through the support located below the pick-up coil. When the plasma is higher, Fig.4(b), the halo current needs to go around the pick-up coil to close its poloidal path. At this stage, the current collected by the IUIWP tile is less or opposite; as the halo current is first tangent and then on the other side of the confined plasma. This interaction with the moving plasma also helps explaining why the dump plate pick-up coil systematically measures less current than the IUIWP pick-up coils. In fact, also in the later stages of the disruption, part of the current that goes around the IUIWP coils does not encircle the coil behind the dump plate.

The ASDEX Upgrade bottom divertor is equipped with 90 shunts distributed in poloidal and toroidal arrays. Such a good distribution allows the measurement of very local asymmetries and the observation of the halo current footprint on the divertor. The halo fraction in ASDEX Upgrade can be as large as 50%, and it scales with the amplitude of the plasma vertical displacement during the disruption, similarly to what is observed at JET. Like in JET the halo TPF of ASDEX Upgrade disruptions is larger when the cylindrical safety factor reaches low values. However, while in JET the cylindrical approximation boundary safety factor (q_{cyl}) has to decrease to ~1 in order to have large asymmetries, a q_{cyl}~2 triggers halo asymmetries in ASDEX Upgrade.

In ASDEX Upgrade, high q_{95} density limit and VDEs typically generate asymmetries in the halo current. In disruptions with strong MHD activity, hardly any asymmetry has been observed, suggesting that the MHD activity prevents the plasma from reheating and developing a configuration that could lead to the n = 1 structure [12]. In shots where the n = 1 structure would be expected, this can be suppressed by the injection of a killer pellet, as reported also for DIII-D [13].

Over 150 individual halo detectors are fitted in MAST [14]. All the current sources and sinks have been identified. Generally, in downward events, most of the halo current is collected at the bottom of the centre column (70-80%) and on the inner target (20-30%) and leaves the vessel at the screen of the outer poloidal field coil and at the rib limiters.

MAST halo current data have been compared to the ITER database (Fig.1) as in [14]. The maximum halo current fractions are similar to those observed in conventional aspect ratio tokamaks. However, under normal spherical tokamak operations, with plasma current above 350kA, halo current fractions above 25% have not been observed. Large halo current fractions are seen at low plasma currents, usually associated with large aspect ratio, and fractions up 85% have been produced in experiments where the plasma was driven highly unstable by ramping down the poloidal field currents. Comparison of the peaking factor at four poloidal positions shows a general trend for the TPF to be higher outboard. This can be partly explained in terms of the increased differences in poloidal to toroidal path lengths at larger radius (i.e. toroidal path shorts out the asymmetry). Measurements carried out during the MAST divertor biasing experiment [14] suggest that during VDEs, the plasma acts more as a voltage source than a current source when generating halo currents. Therefore by altering the resistance of the current path it is possible to limit these currents.

3. RUNAWAY ELECTRONS

Depending on the electron temperature and density, runaway electrons can be generated by the loop voltage of a disruption. The runaway beam becomes dangerous when it interacts with the in-vessel components and the vessel walls (causing melting of metals). A good understanding of the RE phenomenology improves the chances of learning how to cope with (or avoid) runaway electrons in operation at high plasma current, where they are most likely.

In the original survey of JET shots with RE production [15] the variations in behaviour caused by different configurations (including carbon and beryllium limiters) were identified and examples of discharges with very long runaway tails given, and subsequently analysed [16, 17]. After the installation of the divertor, rather few discharges had long runaway tails and this is attributed to the more vertically unstable plasma columns caused by the non-symmetric configuration [18].

A recent and more detailed examination of the hard X-ray emission following disruptions showed that many discharges had some spontaneous runaways even though the characteristic plasma current plateau did not develop. In the following the integral of the fast sampled ^{235}U fission chamber current [19] during the disruption is taken as a measure of the presence and magnitude of RE beams. In Fig.5, a survey of a large number discharges shows that runaways occur after a disruption when the value of Bt exceeded the threshold of 2T similarly to JT-60U [20] and TS [21]. The JET data show no clear threshold on the value of the boundary safety factor, which is instead present in the JT-60U data. In addition, the time integral of the HXR current increases by two orders of magnitude as the toroidal field goes from 2T to 3.5T; a similar enhancement in the strength of the RE population has been observed in FTU [22]. Analysis of a number of disruption with runaway electrons shows that the time integral of the ^{235}U chamber current has an upper limit which scales with the initial plasma current decay rate. Although the chances of surviving (large hard X-ray integral) are better at low elongation, no trend in RE generation has been found with the elongation.

A systematic plasma current scan at B_t = 3T and 3.4T on low elongation (limiter) deliberate

(argon puffing) disruptions has been conducted to further the understanding of RE production and to try to develop control scenarios. At both fields the generation is maximum at ~2MA and drops to almost zero at higher and lower currents. It is thought that runaway beam generation does not occur at low plasma currents as the electric field is too low; while at high currents, magnetic fluctuations may prevent their formation [23]. Fig. 6 shows one of these dedicated discharges, pulse 53786, which produced a very long RE tail. Diffusion losses at these toroidal field and plasma current (3 T and 2 MA) do not seem to play a significant role in the destruction of the RE beam. In fact, once the plateau is reached the current is kept constant, until the beam crashes into the vessel wall, as indicated by the bursts in the neutron and γ-rays measurements. There are delays between the loop voltage peak and the observation of γ-rays and of neutrons. This can be understood taking into account the time development of the electron energy. When there is an appreciable number of runaway electrons with an energy of ~1 MeV, γ-rays will be observed; whereas neutron production requires the (g,n) threshold of ~10 MeV to be exceeded.

Pulse No: 53786 has been analysed with a 0D model [23] and subsequently with the ARENA code [3], which solves the relativistic drift kinetic equation for electrons in toroidal geometry. Crucially, both primary (Dreicer) and secondary (avalanche) runaway production are taken into account, and the evolution of the toroidal electric field is calculated self-consistently in ARENA. The current carried by the runaways thus modifies the electric field responsible for the runaway production in the first place, making the dynamics non-linear. Background plasma parameters such as electron density and temperature are specified as input parameters to the code, and the thermal quench is modelled by letting the electron temperature fall in a prescribed way, e.g., $T_e(r, t) = T_0 + (T_1 - T_0) \exp(-t/t_0)$, where T_0 and T_1 are the pre- and post-disruption temperatures, respectively. This causes the resistivity to increase and the inductive toroidal electric field to rise, triggering runaway generation: first by primary generation and later by the avalanche mechanism [24, 25]. This limits the further growth of the electric field and eventually brings it down to values where no more runaways are generated.

Figure 7 shows an example of such a simulation with parameters chosen to match JET Pulse No: 53786. The density profile was taken to be ne = $[1 - 0.9 (r/b)^2]^{1/2} \times 5 . 10^{19}$ m^{-3}, the pre- and post-disruption temperatures were $(T_0, T_1) = [1 - 0.9 (r/b)^2]^2 \times (1.4\text{keV}, 20\text{eV})$, where b = 1 m is the radius of the plasma-vacuum interface, and the time scale for the thermal quench was t_0 = 1ms. There is good agreement between the computed electric field and the measured (at ~1.8m radius) toroidal voltage (Fig.6). The runaway production commencing 4 ms after the onset of the thermal quench is initially very fast and due to primary generation. This triggers a secondary avalanche, which lasts for about 5 ms. As predicted by theory [24, 25], most runaways are generated by the avalanche, and the process is quite sensitive to the electron density. At higher densities, runaway production is slower and less effective, so that a smaller fraction of the current is converted to runaways.

The runaway electrons energy spectrum consists of two parts: a drawn-out tail and a high-energy

"bump". The bump is mainly made up of primary (Dreicer) runaway electrons, while the tail represents secondary (avalanche) electrons. The Dreicer runaway electrons are produced first and are therefore accelerated longest and reach the highest energy, while the avalanche electrons have lower energy. The energy of the Dreicer runaway electrons is consistent with the flux change available for their acceleration [26]: ~1Vs at the plasma axis gives ~15MeV.

The code can also be run with radial diffusion (caused by magnetic fluctuations) acting on the runaways, which tends to suppress runaway production [27]. With a diffusion coefficient equal to the Rechester-Rosenbluth value [28], a significant effect is observed if the magnetic fluctuation level exceeds $\delta B_r/B \sim 10^{-2}$, just above to the upper end (5×10^{-5}) measured in the fixed-Bt current scan experiments [23].

4. HEAT LOADS

Disruption heat loads are crucial to the survival of the divertor of any next generation machine. If, as currently believed, all the thermal energy of the plasma is deposited on the divertor on a limited area (only three times the steady state area), the suitable divertor materials are not compatible with low tritium inventory requirements.

The JET divertor is observed by an infra-red (IR) camera, which detects photons in the 3-5mm region [29]. The detector collects data on four 2D sub-arrays (64x64 pixels each) at a rate of ~20ms/ lines. The spatial resolution is between 5 and 7mm. The endoscope is located at the upper limiter guide tube of octant 4 (about 25cm above the midplane). The field of view is split into two tangential views of the inner and outer divertor, so that both strike-points are 10 visible in most plasma configurations. The IR data may suffer from the relative displacement (a few cm's) between the endoscope (leading to an enlarged footprint) and the target. In addition, the sampling rate is such that very few points describe the disruption power pulse (leading to a possible underestimate of the deposited energy).Embedded in the divertor target tiles are ~40 thermocouples (TCs) [30]. These are fitted 10mm below the plasma facing surface, evenly distributed poloidally, as to provide a reasonable poloidal profile of the disruption energy distribution on the divertor. While there is only one toroidal location viewed by the IR camera (oct. 4-5), the TCs are distributed over several of the 24 divertor modules.

The total energy radiated during the disruption can be estimated using the JET bolometry [31], which has a sampling rate of 50Hz. A wide-angle camera was temporarily connected to a fast acquisition system in 2003.

Disruptions which fit the requirements of the ITER-relevant classification [32] have been identified among those occurred in the 2002-3 operation, and those with the most diagnostics available analysed in some detail. In most of the disruptions the sum of the radiated energy (which includes also the divertor) and the TC energy is less than the pre-disruption energy. This is representative of the typical JET energy account during disruptions. The energy not found in these sinks can be exchanged with the poloidal field coils and the passive structures [33] or conducted elsewhere in the vessel.

Detailed analysis (TC and IR) of limiter density limit disruptions can be found in [33], here it is only recalled that this type of disruption tends to produce runaway electrons and that when this happens the heat loads (as seen by the TCs) can be toroidally non-uniform. Density limited or collapsed internal transport barriers (ITBs) are the only other disruption type systematically prone to RE generation. Even if not apparent in the table, because the chosen discharges are at a too low toroidal field (see Section 3), density limit disruptions are more likely to give rise to RE, since their loop voltage is higher (the current quench is faster).

The power footprint on the diverotr of the H-mode density limit disruption in Fig.8 is very similar to the previous ELMs. Only one third of the pre-disruption thermal energy is found on the divertor. This event is representative of the majority of JET H-mode disruptions as far as the divertor heat loads are concerned.

In the locked mode disruption of Fig.9 over two thirds of the thermal energy are lost in ~300ms before the major disruption: from 3.6MJ to 1.0MJ, while ~1MJ is still injected by the neutral beams. This slow energy loss is associated to the presence of MHD activity. This typically occurs in low-q operation or following an increase of edge impurity, both lead to an unstable current profile with the $q=2$ surface just outside a steeper than normal current gradient, which is NTM unstable. During the whole event the IR estimates an energy deposition of ~3.5MJ, of which ~1MJ is lost at the concluding disruption: a close match to the thermal energy lost by the plasma. Since the magnetic energy is ~13MJ and the radiated energy only ~8MJ, in total 6MJ are not accounted for (over 30%). The power footprint is wider at the disruption than during the locked mode, and already the locked mode footprint is wider than the equilibrium one.

ITB collapse discharges are associated with a fast growing, rotating, disruptive, $m=2/n=1$ kink mode. The $n=1$ mode can be observed with Mirnov probes [34] and the poloidal structure with electron temperature measurements. The electron temperature measurements also show non-linear ballooning modes superimposed on the outer kink, similar to previous observation in TFTR [35]. The ballooning mode pushes a segment of a central field line out into the outer plasma, ejecting hot plasma into the scrape off layer or onto the walls. In some ITB collapse disruptions, Langmuir probes, both at the divertor and on the outer poloida limiter, register an interaction during thermal quench. Although the data in Fig.10 is not quantitative, the divertor signal is similar to that seen during ELMs, while the limiter signal is not saturated during ELMs. This indicates that the X-point is not lost at the thermal quench and that substantial interaction on the outer poloidal limiter is taking place. Fig.10 also shows one of the few fast sampled disruption radiation energy waveforms. Even if calibration for this signal is not available at the moment, it is clear that radiation starts slowly at the thermal quench and that a significant amount of energy is lost through this channel only during the current quench.

The analysis of JET disruption heat loads suggests that the ITER assumptions on the divertor may be too conservative, while the energy lost to the main chamber should studied in more detail.

5. DISRUPTION MITIGATION

The aims of disruption mitigation are:

- to reduce the amount of energy conducted to the divertor;
- to reduce poloidal halo currents, and related vessel stresses and in-vessel components electromechanical loads;
- to increase the background density so that RE production is prevented.

Halo currents and vessel forces are reduced by operating near the neutral point. In addition, working near the neutral point gives as a longer intervention time to activate disruption amelioration techniques (in particular to avoid runaway electrons). Full exploitation of disruption mitigation will be greatly assisted if neural networks, able to reliably predict the approach of a fatal plasma instability, are developed. Neural networks have already been routinely employed to trigger killer pellets [36] and could be used for high pressure gas jets too, as long as the prediction is available early enough for the mitigation technique to be effectively applied.

5.1 NEUTRAL POINT EXPERIMENTS

Fast axisymmetric plasma disturbances create an imbalance of forces between external currents and the plasma, which can cause the plasma to move vertically in a preferential direction (i.e. upward or downward). There is a position for the plasma current centroid where ideally this imbalance is zero. When a given perturbation at a given instant t_0 excites the (axisymmetric) unstable vertical mode with an initial vertical displacement δz_0, the plasma vertical displacement δz evolves exponentially as $\delta z = \delta z_0 e^{\gamma(t-t_0)}$, where g is the growth rate of the vertical instability. Assuming the quantity dz0 is a function of the initial plasma centroid vertical position where the instability is excited, which changes sign, the neutral point (NP) is the vertical position at which δz_0 vanishes.

Some dedicated experiments performed on JET, and related simulations, demonstrate the existence of a neutral point for density limit disruptions of a plasma, specially designed to be set at different vertical equilibrium positions without altering the shape. The plasma moves upwards (downwards) when the disruption is triggered with the plasma below (above) the NP. The CREATE_L linearized plasma response model [4] applied to such configurations is able to predict and explain the most significant qualitative features of the experiment [37]. This provides a valuable validation of the CREATE_L code.

The growth rate does not significantly vary among the configurations analysed. Therefore, the location of the neutral point is determined by plotting, Fig.11, the vertical displacement (dz_p) of the plasma current centroid after a given time interval (3ms) from the thermal quench (Hα spike), as a function of the initial plasma vertical position. The quantity dz_p depends almost linearly on the initial vertical plasma position, and changes sign around ≈20cm. The directionality is opposite to the intuitive one. The directionality of ASDEX Upgrade disruptions [38] deviates from intuitive forecasts, but this deviation can be explained taking into account the dynamics of the current profile. A large number of bottom divertor configurations positioned well above the neutral point computed

via TSC [39] move downward at the disruption, while some go upwards. TSC simulations show that the slower is the drop in internal inductance, the weaker is the drag towards the X-point, so that the actual neutral point is at a higher position. The dependence on the internal inductance is a reflection of the fact that the neutral point, analytically, is a function of the plasma magnetic configuration and of the disturbance leading to the plasma disruption.

5.2 HIGH PRESSURE GAS PUFFING IN JET

Only two gas injection valves can operate at relatively high pressure (2.5 bar) and on short time scales at JET. The maximum amount of injected impurity particles in <50 ms is ~9×10^{21}. Three gases have been employed: helium, neon and argon. None of these had an adverse effect on the breakdown of the following discharges. The amount of injected helium had to be limited in order to avoid spontaneous regeneration of the divertor cryopump (the neutral beam boxes had to be closed for the same reason).

Helium alone has been successfully used to prevent RE formation [33] by pre-emptive puffing during impurity induced limiter plasma density limit disruptions at favourable toroidal field and plasma current (3T and 2MA). The helium puff prevented RE generation for at least two reasons: the background density was higher and the plasma current decay was slower.

In X-point deliberate VDEs, the main effect of helium injection was to slow down the disruption, leading to overall more demanding electromagnetic loads (e.g. vessel forces [33]). Fig.12 shows how puffing neon or argon is sufficient to at least transform a potential VDE into a density limit disruption. Obviously this has an effect on the electromagnetic loads, which are significantly decreased. In Fig.13 the product of the halo current fraction times the TPF is plotted versus the time interval between thermal quench and a plasma vertical displacement of 10cm. There is hardly any correlation between the gas used (or its reservoir pressure) and the halo parameter; the latter seems to depend only on the timing of the thermal quench with respect to the lost of vertical equilibrium position. On the other hand the effect on the electron temperature of neon and argon, as puffed in these discharges, is rather different. While the drop in electron temperature is much faster than in a "normal" disruption when neon is puffed; there is no significant change in the electron temperature dynamics when argon is puffed. The argon-puffed thermal quench is better explained as a slow radiative collapse instigated from the highly radiating edge plasma that eventually just shrinks the current profile to an unstable position. It is unclear how much argon is actually available to the central plasma, as the gas beam could have degraded after injection: both the argon and the neon gas puffs take at least 20 ms before becoming effective at the plasma centre. This is equivalent to an average speed of 75m/s, less than half the sonic speed of argon or neon.

Simulations have been carried out using KPRAD [40] to find effective gas parameters that match measured disruption times in a triggered VDE with a neon gas puff. The plasma thermal quench occurs ~23ms after the initiation of the neon gas puff. The current quench decay time is ~6ms. The neon is provided at low pressure, so it is promptly ionised in the plasma edge and pinch/diffuse into

the central plasma on a time scale set by the injection rate and the cross-field plasma transport. In the KPRAD simulation, the neon is assumed uniformly distributed through the plasma. A constant neon injection rate into the plasma is assumed over 50ms. In the attempt to simulate the effects of edge screening, the injection rate and the initial charge state of neon are scanned. The thermal quench time can be obtained by reducing the injection rate to a fifth of the experimental value. At this injection rate, experimental results are consistent with an initial charge state of ~7, representative of a situation dominated by plasma transport of the neon. Therefore, KPRAD modelling suggests that the JET neon gas puff does not penetrate effectively as a neutral.

Although the JET gas puff experiments have not been successful (argon and neon did not penetrate effectively), these experiments should be repeated, when a suitable injection valve is available, as to produce conditions closer to those in DIII-D and enable size extrapolation towards ITER. Assuming that the parallel field is not affected by the amount of injected impurity, as shown in [41], to ensure RE prevention the total electron density (that is bound and free electrons) needed to increase the critical field ($E_c = mcv/e \sim 10^{21} \, n_{e,tot}$) as to match the computed parallel field of 10V/m (Fig.7) is ~10^{22} m^{-3}, equivalent to ~8×10^{22} neon atoms. This value is similar to the one required in DIII-D and ITER [41], and ten times larger than the one presently achievable at JET (8×10^{21}).

5.3 DISRUPTION MITIGATION IN DIII-D, TEXTOR AND ASDEX UPGRADE

In DIII-D recent disruption mitigation experiments [41] saw the reduction (or elimination) of thermal loading of the divertor surfaces, of poloidal halo currents and of runaway electrons generation. High-pressure jets of neon and argon reach the centre of the plasma as neutral gases at sonic velocity. The fast valve, fitted on a 70 bar reservoir, releases ~4×10^{22} particles in 2-5ms, achieving an impurity density ~35 times larger than the typical electron density (3×10^{19} m^{-3}). When the target is a stable plasma, no significant MHD activity is observed until a large amount of radiation comes from the core, where the impurity has been deposited. The electron temperature drops in ~0.2ms and the plasma current decay starts promptly. More than 95% of the plasma stored energy is radiated. The gas injection has no adverse effect on any pumping system and there are no breakdown problems for the following discharge. The plasma control system has been programmed to inject neon when a VDE is detected in discharges where the event is deliberately initiated by disabling the vertical control system. In these events the energy deposited on the divertor is reduced by a factor of 2 for the inner target and a factor of 5 for the outer target with respect to non-mitigated events. Also the poloidal halo currents are reduced, because the plasma current decays more rapidly than the plasma movement into the wall, so keeping the boundary safety factor higher than in non-mitigated disruptions.

Differently from the use of killer pellets [9, 13], no significant population of runaway electrons has been observed after killer jets in DIII-D. Both techniques cause rapid radiative cooling and current quench, but the gas jet injects ~100 times the number of atoms (although the number of free electrons is only moderately higher).

A fast valve has been developed in TEXTOR [42] in order to prove runaway suppression by fast helium puffing. This was tested on low density runaway discharges. The runaway electrons start

10

interacting with the injected helium within 0.5 ms of the opening of the valve and are quickly slowed down. The hard X-ray detectors show that the runaway electrons are not expelled to the wall at their original (high) energy, therefore they must lose most of their energy interacting with the injected helium.

A fast valve similar to the one used in TEXTOR has been developed for ASDEX Upgrade [43] and used in a set of feed-forward disruption mitigation experiments carried out on healthy plasmas using helium, neon and argon [44]. The measured current quench rate of limiter plasmas goes from ~20MA/s with helium to 60-80MA/s with neon and argon; the delay between the gas reaching the plasma edge and provoking the disruption was 12ms for helium, 4ms for neon and 2ms for argon. Argon caused some contamination, while helium was inefficient. Runaway electrons were observed in a few discharges with density lower than $4 \times 10^{19} \, m^{-3}$ and toroidal field higher than 2 T. Similarly neon pellets [45], in early mitigation experiments, although effective with respect to heat and electromechanical loads, were later found to give rise to runaway electrons. In contrast silicon or titanium powder in molten polyethylene killer pellets [36] did not give rise to long-lived runaway electrons and were able to eliminate the energy deposited on the divertor at the thermal quench and half the poloidal halo current.

CONCLUDING REMARKS.

Data from the improved halo current measurement system confirmed the historical scatter of JET [f, TPF] values. This is consistent with having less demanding halo current design criteria coming from large machines and confirms the ITER assumptions.

In JET, like in JT-60U and TS, there is a toroidal field threshold below which disruption runaway electrons are not observed. In addition, using the time integral of the fission chamber current during disruptions, it has been shown that the RE beams are stronger at higher toroidal fields. Modelling of a discharge with sustained runaway electron beam shows that most of the runaway current is carried by avalanche electrons, in agreement with the ITER predictions.

In JET, divertor deposited energy and radiated energy are not sufficient to account for the total pre-disruption plasma stored energy. The missing energy can be exchanged with the poloidal field coils and the passive structures [33] or conducted elsewhere in the vessel, and in fact the outer poloidal limiter, as well as divertor, Langmuir probes register current spikes during the thermal quench.

In H-mode disruptions the divertor power pulse is not worse than preceding ELMs, typically depositing only a small fraction of the plasma thermal energy on the divertor. When the energy deposited on the divertor is a large fraction of the plasma thermal energy, the footprint is wider than in normal operation. Based on JET results, the ITER design guidelines appear conservative and the use of materials such as tungsten in the divertor may feasible.

Disruption mitigation can be achieved with mixtures of techniques. Operation at the neutral point, which alone already reduces significantly halo current loads, is helpful if fast gas jets have to be employed to ameliorate runaway electrons, as a longer intervention time is available since the vertical position is lost more slowly. Killer pellets are suitable for routine operation in conjunction

with a neural network [36] and are efficient in reducing the electro-mechanical forces and the energy deposited on the divertor, but they tend to produce runaway electrons. To avoid RE generation the density needs to be increased, that implies the number of injected particles has to be large. This is achieved with high pressure gas jets, which are more technologically demanding than killer pellets, and have been successfully tested in DIII-D and to lower specification in ASDEX Upgrade and JT-60U.

Recent JET data confirms the ITER design guidelines for halo currents. The ITER divertor disruption heat loads assumptions may be too conservative. As at JET some energy is deposited in the main chamber, this disruption heat load sink should be further investigated. Disruption mitigation techniques applicable to ITER have been successfully tested in DIII-D, ASDEX Upgrade and JET.

ACKNOWLEDGEMENTS

REFERENCES

[1]. ITER Physics Basis 1999 Nuclear Fusion **39** Chapter 3 Section 4

[2]. V. Riccardo et al., Refurbishment of the JET halo current diagnostics, accepted for publication in Fusion Engineering and Design

[3]. L.G. Eriksson, P Helander, Simulation of runaway electrons during tokamak disruption, for publication in Computer Physics Comm.

[4]. R. Albanese, F Villone, Nuclear Fusion **38** (1998) 723

[5]. P. Andrew et al., Proc. 17th IEEE/NPSS Symposium on Fusion Engineering (1997) 108

[6]. Granetz et al., Nuclear Fusion **36** (1996) 545

[7]. Granetz, Disruption halo currents with C-Mod's new divertor, APS-DPP, Orlando (2002)

[8]. P. Knigth et al., Nuclear Fusion **40** (2000) 325-337 20

[9]. Kellman et al., in Fusion Energy 1996 (Proc. 16th Int. Conf. Montreal, 1996), Vol.1, Vienna (1997) **739**

[10]. V. Riccardo, Fusion Science and Technology **43** (2003) 493

[11]. D. A Humphreys, AG Kellman, Physics of Plasmas **6** (1999) 2742

[12]. G Pautasso et al., 28th European Physical Society Conference on Plasma Physics and Controlled Fusion, Madeira (2001) P-1.005

[13]. T. E Evans et al., Journal of Nuclear Materials **241-243** (1997) 606

[14]. R Martin et al., 29th European Physical Society Conference on Plasma Physics and Controlled Fusion, Montreux (2002) P-1.053

[15]. G. R. Harris, Comparisons of the Current Decay during Carbon-bounded and Beryllium-bounded Disruptions in JET, JET-R(90)07 (1990)

[16]. J. Wesson, R D Gill, M Hugon, F C Schüller et al., Nuclear Fusion **29** (1989) 641

[17]. R. D. Gill, Nuclear Fusion **33** (1993) 1613

[18]. R. D. Gill et al., Nuclear Fusion **40** (2000) 163

[19]. O. N. Jarvis, Treatment of the KN1 data channels, JET-TN(87)04 (1987)

[20]. R. Yoshino et al., Plasma Physics and Controlled Fusion **39** (1999) 313

[21]. G. Martin, Control of runaway electrons created during major disruptions, IAEA TCM on Avoidance and Control of Tokamak Disruptions, Culham, 1991

[22]. F. M. Poli, B. Esposito, G. Maddaluno, Disruption generated runaways in FTU high field tokamak, 43rd American Physics Society Conference, Long Beach (2001) GP1.063

[23]. R. D. Gill et al., Nuclear Fusion **42** (2002) 1039

[24]. M. N. Rosenbluth and SV Putvinski, Nucl. Fusion **37** (1997) 1355

[25]. P. Helander, L. G. Eriksson and F. Andersson, Plasma Phys. Control. Fusion **44** (2002) B247

[26]. O. Jarvis et al., Nuclear Fusion 28 (1988) 1981

[27]. P. Helander, L.G. Eriksson and F. Andersson, Phys. Plasmas **7** (2000) 4106

[28]. A.B. Rechester and M. N. Rosenbluth, Phys. Rev. Lett. **40** (1978) 38

[29]. T. Eich et al., Journal of Nuclear Materials **313-316** (2003) 919

[30]. V. Riccardo et al., Plasma Physics and Controlled Fusion **43** (2001) 881

[31]. KF Mast et al., Review of Scientific Instruments **56** 5.2 (1985) 969

[32]. A. Loarte, Disruption Working Group Public Web Site (2003)

[33]. V. Riccardo et al., Plasma Physics and Controlled Fusion 44 (2002) 905

[34]. G. T. Huysmans et al., Nuclear Fusion **39** (1999) 1489

[35]. Fredrickson et al., Physics of Plasma **3** (1996) 2620

[36]. G. Pautasso et al., Nuclear Fusion **42** (2002) 100

[37]. F. Villone, Neutral point detection in JET, accepted for publication in Fusion Engineering and Design

[38]. Y.. Nakamura et al., Plasma Phys. Control. Fusion, Vol **44** (2002) 1471

[39]. S. C. Jardin et al., Journal of Computational Physics **66** (1986) 481

[40]. D. G. Whyte et al., 24 th European Conference on Controlled Fusion and Plasma Physics (1997) 21A, 1137

[41]. D. G. Whyte et al., Disruption Mitigation using High-Pressure Noble Gas, Injection on DIII-D IAEA Conference, Lyon (2002)

[42]. K. H. Finken et al., Journal of Nuclear Materials **313-316** (2003) 1247

[43]. A. Savchkov, G Pautasso, KH Finken, G Mank, 29th European Physical Society Conference on Plasma Physics and Controlled Fusion, Montreux (2002) P-3.203

[44]. G. Pautasso et al., 29th European Physical Society Conference on Plasma Physics and Controlled Fusion, Montreux (2002) P-2.051
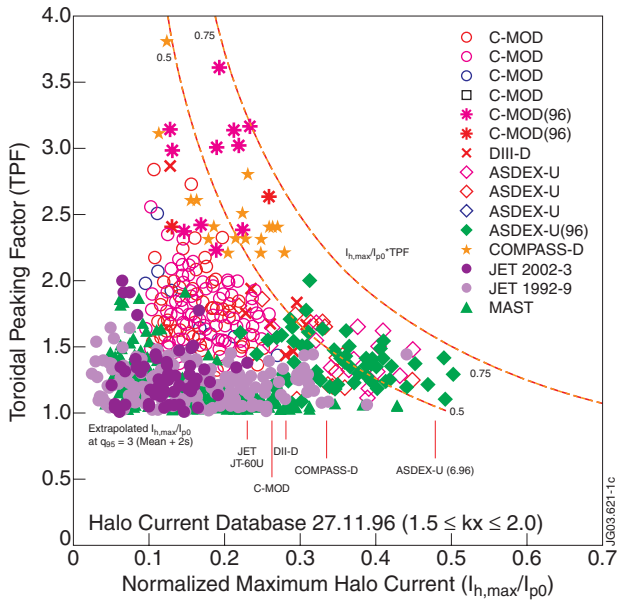
[45].G. Pautasso, Nuclear Fusion **36** (1996) 1291

Figure 1: ITER halo current design data [1] overlaid with 1992-9 and 2002-3 JET and MAST halo data.
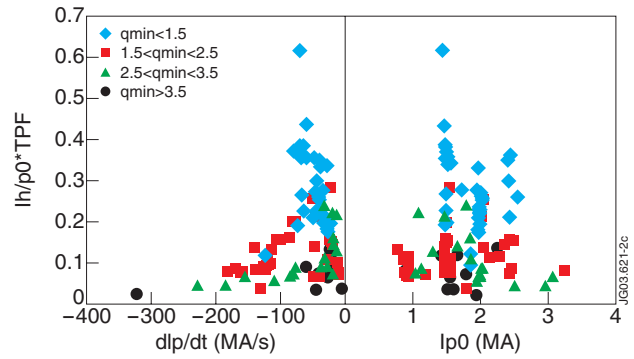

Figure 2: The product of halo fraction and TPF is plotted versus the plasma current quench rate (taken between 95% and 35% of the maximum plasma current) and the pre-disruption plasma current.
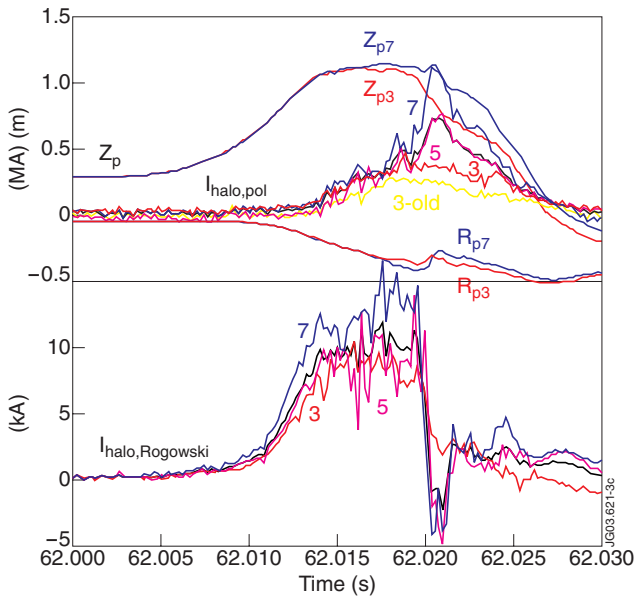

Figure 3: Plasma vertical and radial position and current in two opposite toroidal locations (Octant 3 and 7) for Pulse No: 56817 plotted together with the IUIWP-tile collected halo current (Octant 3, 5 and 7) and the poloidal halo current measured at the IUIWP (Octant 3, 5 and 7) and behind the dump plate (Octant 3)
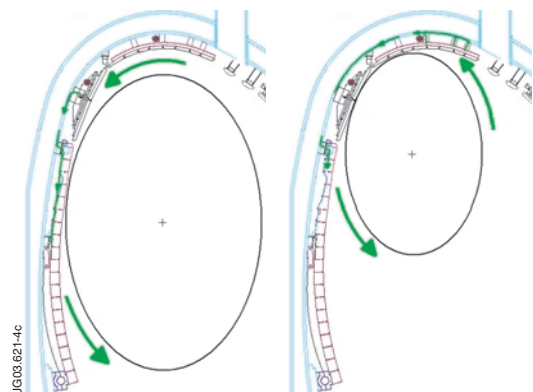
Figure 4: Sketch of the confined plasma interacting with the inner and upper wall in the early (a) and late (b) stages an upward VDE

14
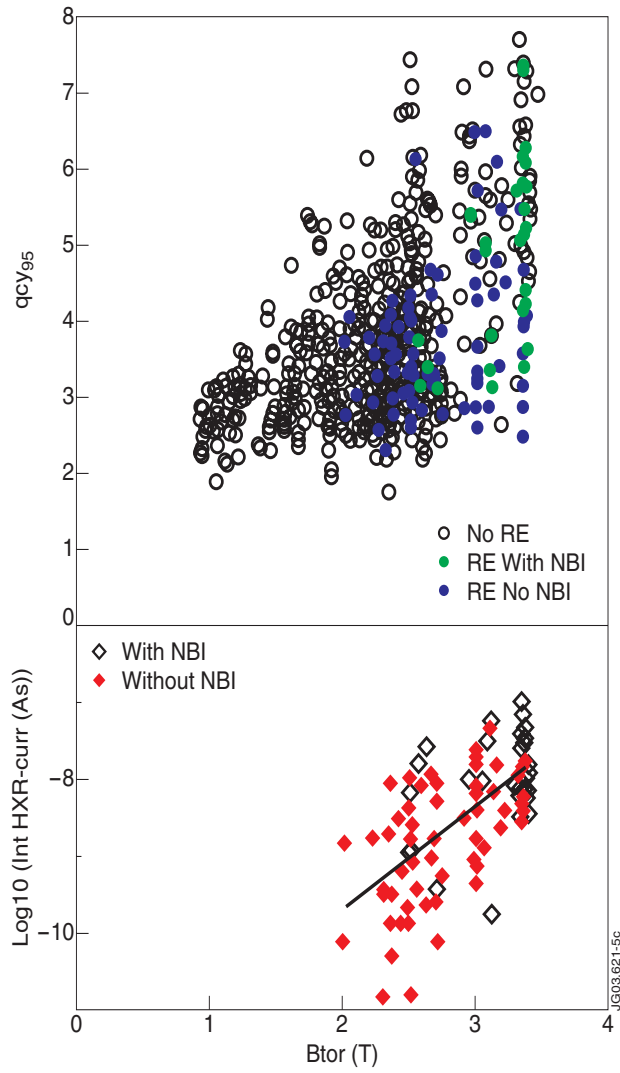
Figure 5: 1998-2003 JET disruption with RE (with and without NBI) are high lighted in the (B_t, q_{95})-space among other disruptions; the integral of the ^{235}U fission chamber increases on average by 2 orders of magnitude as the disruption toroidal field goes from 2T to 3.5T
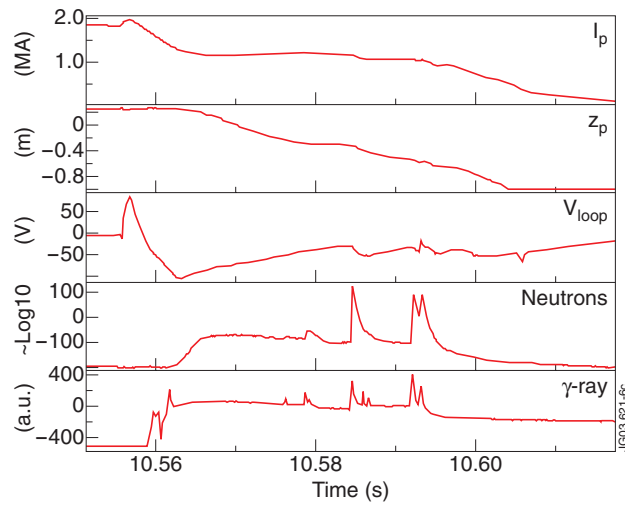
Figure 6: Time traces of plasma current and vertical position, loop voltage, HXR neutrons and γ-rays for Pulse No: 53786
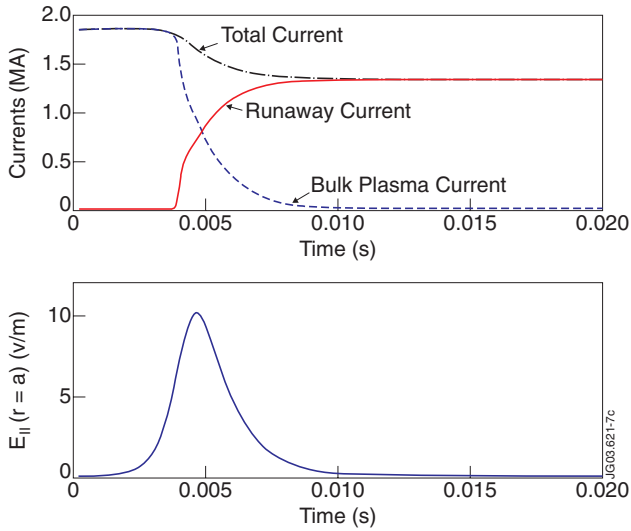
Figure 7: Evolution of the runaway and bulk plasma currents, and the electric field at the wall in an ARENA simulation of JET Pulse No: 53786.
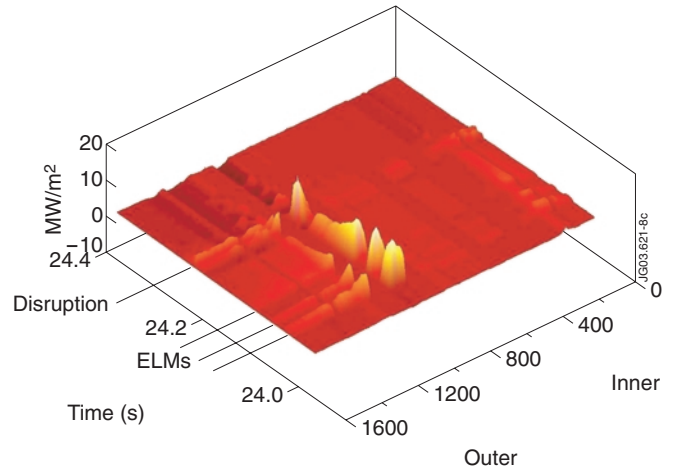
Figure 8: Power density on the divertor during an ELMy H mode density limit disruption (JET Pulse No: 58009)
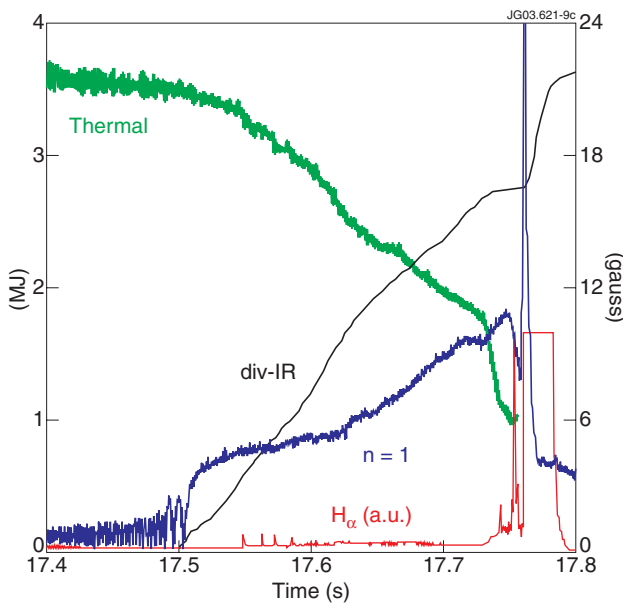
Figure 9: Time traces of the outer divertor Hα, the n=1 mode amplitude, the plasma thermal and the IR divertor energy (integral started when the mode locked) for Pulse No: 59027 (disruptive locked mode).
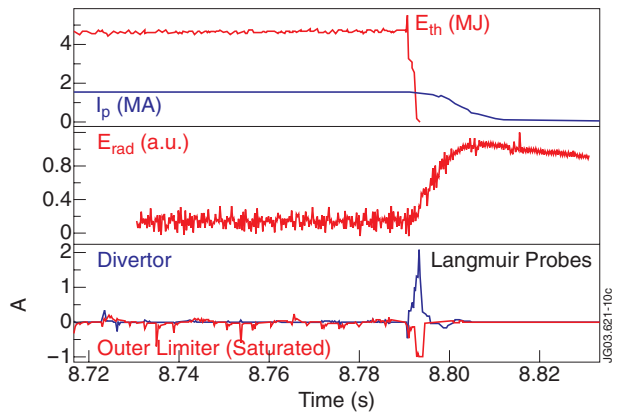

Figure 10: Plasma current, thermal energy, fast sampled radiated energy, poloidal limiter and divertor Langmuir probe currents for the ITB collapse of Pulse No: 58456
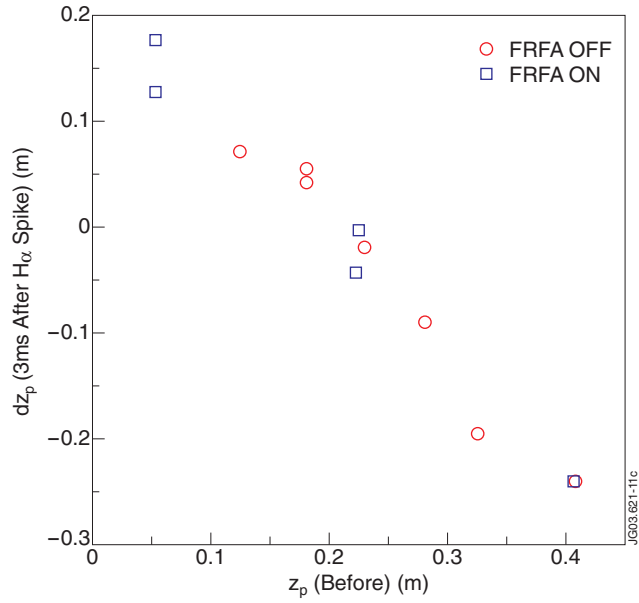
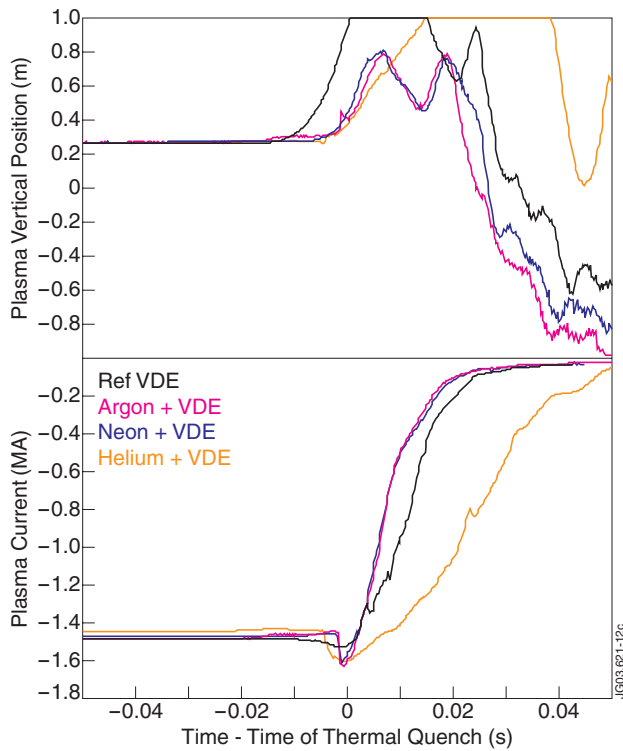*Figure 11: Vertical position displacement as a function of the starting vertical position*

Figure 12: Plasma vertical position (top) and current (bottom) for a reference and three mitigated VDEs
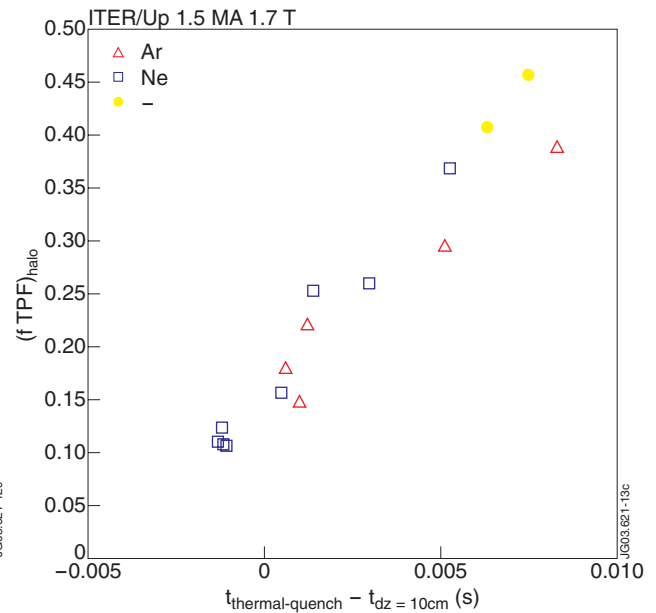

Figure 13: Halo fraction times TPF plotted versus the time difference between thermal quench and a vertical displacement of 10cm for reference and neon or argon mitigated disruptions